Visible emission of hydrogen flames

R.W. Schefer *, W.D. Kulatilaka, B.D. Patterson, T.B. Settersten

Combustion Research Facility, Sandia National Laboratories, Livermore, CA 94551-0969, USA

A B S T R A C T

The common misconception that hydrogen flames are not visible is examined. Examples are presented of clearly visible emissions from typical hydrogen flames. It is shown that while visible emissions from these flames are considerably weaker than those from comparable hydrocarbon flames, they are indeed visible, albeit at reduced light levels in most cases. Detailed flame spectra are presented to characterize flame emission bands in the ultraviolet, visible and infrared regions of the spectrum that result in a visible hydrogen flame. The visible blue emission is emphasized, and recorded spectra indicate that fine spectral structure is superimposed on a broadband continuum extending from the ultraviolet into the visible region. Tests were performed to show that this emission does not arise from carbon or nitrogen chemistry resulting from carbon-containing impurities (hydrocarbons) in the hydrogen fuel or from CO_2 or N_2 entrainment from the surrounding air. The spectral structure, however, is also observed in methane flames. The magnitude of the broadband emission increases with flame temperature in a highly nonlinear manner while the finer spectral structure is insensitive to temperature. A comparison of diffusion and premixed H_2 flames shows that the fine scale structure is comparable in both flames.

© 2009 The Combustion Institute. Published by Elsevier Inc. All rights reserved.

1. Introduction

Although visible emission of hydrogen flames has been addressed in the literature [1–6], a large number of visitors to the Combustion Research Facility at Sandia National Laboratories express surprise when they discover that hydrogen flames are indeed visible to the human eye. Similar comments frequently arise during presentations at meetings regarding our hydrogen flame research program. These numerous responses have led the present authors to address the question of hydrogen flame visibility in this article.

Indeed, examples illustrating the visibility of hydrogen flames are readily available in the literature. For example, Fig. 1 shows a hydrogen flame in a burner that has been studied in collaboration with NASA Glenn [7]. The conditions shown are premixed hydrogen and air at an equivalence ratio, ϕ, of 0.33 and an inlet velocity of 90 m/s. The premixed H_2/air mixture is injected through nine 6.72-mm-diameter holes equally spaced around the inlet plate at the upstream end of a 41-mm-diameter combustor test section. The flames are stabilized in recirculation zones formed by the sudden expansion of gas from the inlet holes into the combustor section. The exposure time is a relatively long 0.6 s, so the bluish color is actually quite faint relative to hydrocarbon (CH_4) flames.

A second example, shown in Fig. 2, is a photograph of a space shuttle launch. Blue emission observed in a similar photograph

was the subject of discussion after the first shuttle launch [6]. The blue color emitted from the H_2–O_2 fueled main shuttle engines can be seen in the lower right quadrant of the photograph. The reactant mixture consists of pure hydrogen and pure oxygen, and thus would seem to rule out the possibility that the blue emission is due to some "contaminant" such as CO_2, which is present naturally in ambient air, or to trace amounts of hydrocarbon contaminants in the hydrogen fuel source.

Naturally occurring visible and ultraviolet flame emission has attracted significant interest in the combustion research community since the first developments in flame spectroscopy in the nineteenth century. Researchers often use chemiluminescence from flame species, such as OH^*, CH^* and C_2^*, as a passive diagnostic. Haber and Vandsburger [8] have proposed that chemiluminescence measurements may provide useful diagnostics in many practical combustion devices where the use of laser-based and physical sampling probes is difficult because of the lack of physical access and the harsh environment. Studies have shown that chemiluminescence emissions can be related to heat release rate, flame structure, and reaction rate [9,10]. For example, the emission intensity ratios of OH^*/CH^* and C_2^*/CH^* were shown by Ikeda et al. [11] to be good markers for equivalence ratio in both laminar and turbulent premixed flames. In this case, it was noted that the CH^* and C_2^* emission resides on a broadband blue continuum, which is attributed to CO–O^*. The fact that careful correction for the contribution of the underlying continuum to the emission measurements is critical, especially at high pressure, underscores the importance of characterizing the structure of the flame emission spectrum.

---

* Corresponding author.
E-mail address: rwsche@sandia.gov (R.W. Schefer).

Fig. 1. Flame luminosity photograph in NASA Glenn hydrogen burner for inlet velocity of 90 m/s and $\phi = 0.33$. Image taken at $f/2.4$ aperture with 0.6-s exposure time.

Haber and Vandsburger [8] emphasize that detailed and accurate chemiluminescence models are necessary for correct interpretation of chemiluminescence measurements. Currently proposed models often do not match experimental data due to uncertainties in the reaction mechanisms. It is clear that the optimization of these techniques and their quantitative extension to other measurements in flames will require a detailed understanding of the kinetic mechanisms involved in flame emissions.

The primary objectives of this article are to examine the notion, even among well-established combustion scientists, that hydrogen flames are invisible to the human eye and to present detailed emission spectra that may provide the data necessary to develop improved chemiluminescence models. In addition to the examples presented in this section of clearly visible emission from typical hydrogen flames, additional photographs of flame emission from laboratory-scale premixed and diffusion hydrogen/air flames will be presented. We will further present detailed flame spectra to characterize the flame emission bands that result in a visible hydrogen flame. The features of the blue emission found in these flames is emphasized, with resolved spectra demonstrating that a structured emission is superimposed on a broadband continuous emission.

2. Experimental

Premixed and diffusion flames were stabilized on an axisymmetric burner. The burner consisted of a 2-mm-diameter nozzle surrounded by a 50-mm-diameter honeycomb that produced an annular guard flow to isolate the central flow from ambient room air. Fuel and oxidizer were metered using calibrated mass-flow controllers, premixed upstream of the burner, and supplied through the center nozzle. For premixed flame conditions, the oxidizer was injected into the fuel sufficiently far upstream to ensure

Fig. 2. Photograph of shuttle launch. Photograph shows blue color for H_2–O_2 fueled main shuttle engines (photo courtesy of NASA). (For interpretation of the references to color in this figure legend, the reader is referred to the web version of this article.)

complete mixing at the nozzle exit. Alternatively, diffusion flame conditions were achieved by flowing pure fuel through the nozzle exit and operating the burner without a guard flow. For the hydrogen fuel, both CP grade (99.0%) and certified ultra-high purity (UHP) grade (99.999%) gases were used. In some cases, CP grade (99.0%) CH_4 was added to the fuel flow to deliberately make carbon chemistry relevant in the flame. For all cases the oxidizer was UHP grade O_2 (99.98%). Either pure nitrogen (N_2) boil-off from liquid nitrogen or high-purity (HP) argon (Ar) was used as a diluent and for the surrounding guard flow. According to the manufacturer's certification, the total hydrocarbon (THC) impurities for the UHP H_2, UHP O_2, and HP Ar were less than 10, 1000, and 3000 parts-per-billion (ppb), respectively.

Flame emission was collected and focused onto the vertical entrance slit of a 0.25-m imaging spectrograph (Oriel MS260i) using two 50-mm diameter, +150-mm focal length BK7 achromatic doublets that were anti-reflection coated for 400–700 nm. After the first achromatic doublet, the nearly collimated light was reflected through a periscope containing two 100-mm diameter silver mirrors to reach the height of the entrance slit of the spectrometer. To collect survey spectra, including the UV region, the BK7 achromatic doublets were replaced with a UV-grade fused silica lens. The width of the spectrometer entrance slit was set to 50 μm. Two diffraction gratings (300 and 2400 lpmm) were used for the current experiments. The 300-lpmm grating produced a spectral
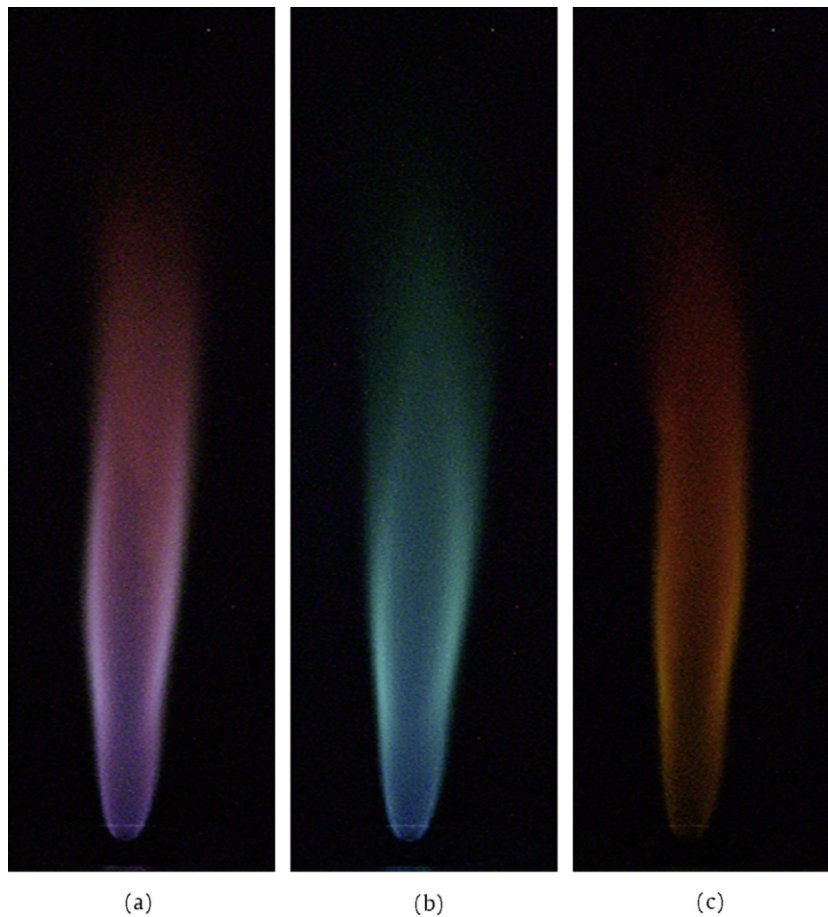
Fig. 3. Direct flame luminosity photographs in a laminar, diffusion H_2-jet flame. (a) Unfiltered, $f/2.4$ aperture; (b) short-wavelength pass filter with 550 nm cutoff wavelength, $f/2.4$ aperture; (c) long-wavelength pass filter with 530 nm cutoff wavelength. Images taken at $f/2.4$ aperture with 90-ms exposure time. Fuel jet exit velocity is 47 m/s with a coflow air velocity of 0.57 m/s. Reynolds number = 837.

resolution of approximately 2 nm and was used for acquiring survey spectra. The spectral resolution produced by the 2400-lpmm grating was approximately 0.2 nm. The spectrally dispersed light was imaged onto an intensified charge-coupled device CCD camera (Andor Model DH520-25F-03) mounted at the exit plane of the spectrometer. One dimension of the CCD image corresponded to wavelength and the other corresponded to distance along the radial direction in the flame. Spectrally resolved emission profiles were obtained by integrating the CCD image along the spatial direction. The integrated spectra corresponded to the emission that was collected from an approximately 5-mm × 50-μm region in the flame. This collection region is shown by the white line in the flame photograph in Fig. 6. In general, the center of the collection volume was located approximately 12 mm above the nozzle.

The wavelength calibration and spectral responsivity of the detection system were obtained for both gratings at all grating angles used in the experiment. Atomic emission lines from mercury and hydrogen and the second harmonic of a single-mode Nd:YAG laser were used in the wavelength calibration procedure. The relative spectral responsivity was measured using a NIST traceable tungsten lamp. This calibration accounted for the spectrally dependent collection efficiency of the lenses, mirror reflectivity, grating efficiency, and the responsivity of the intensified camera. The wavelength and responsivity calibrations were applied to all flame spectra.

3. Results

3.1. General emission features

Shown in Fig. 3 are digital photographs of a laminar, diffusion H_2-jet flame into air. All photographs were taken with a Sony DSC-D700 digital camera (1344 × 1024 pixel format) using an exposure time of 0.09 s and a $f/2.4$ aperture. The photograph on the left was obtained using unfiltered flame emission. The flame luminosity in middle photograph was filtered using a 550-nm short pass filter (Melles Griot 03SWP015 fused silica with 85% average transmission between 375 and 540 nm), and the flame emission on the right was filtered using a 530-nm long pass filter (Schott colored-glass sharp-cutoff filter OG530). Both the blue and red/orange components of the luminescence are clearly seen.

Fig. 4 shows flame luminescence photographs of a laminar, premixed H_2–air jet flame. Photographs are shown for equivalence ratios of $\phi = 1.0$, 0.8, 0.7 and 0.62. At the higher equivalence ratios (Figs. 4a and 4b), two regions are clearly visible. The upstream region, which extends approximately one-third of the total flame length, appears blue. The downstream region appears red. In the two leaner flames (Figs. 4c and 4d), the red downstream region is less visible due to the lower gas temperatures at the leaner conditions.

It is interesting to compare the relative flame luminosities of the H_2 flames and a comparable hydrocarbon flame. All flame images in Figs. 3 and 4 were taken at an aperture setting of $f/2.4$. To achieve the same exposure as in the images of the diffusion flame,
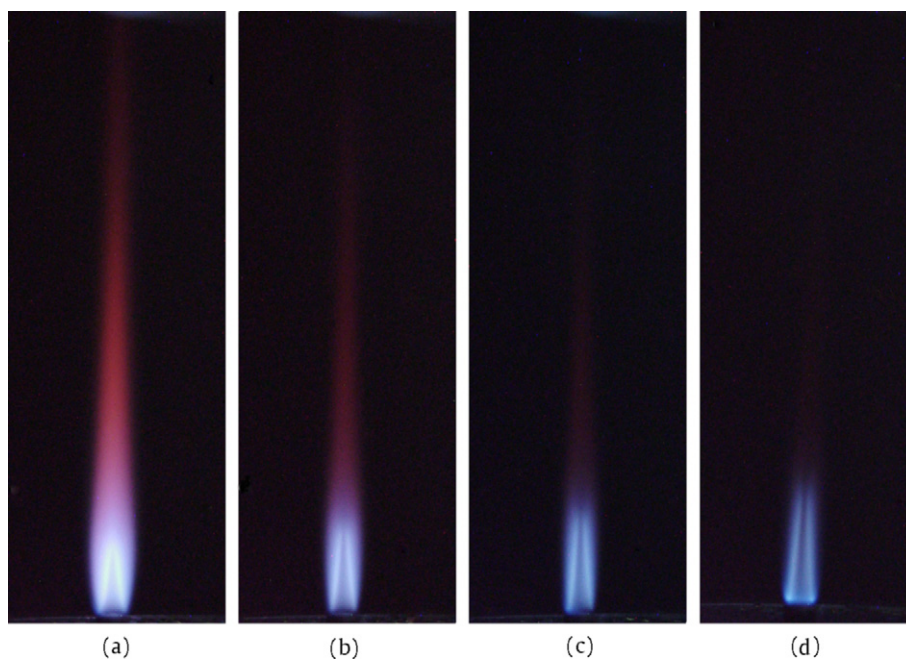
Fig. 4. Flame luminescence photographs of turbulent, premixed H_2–air jet. (a) $\phi = 1.0$, (b) $\phi = 0.8$, (c) $\phi = 0.7$, (d) $\phi = 0.62$. Images taken at $f/2.4$ aperture with 4-s exposure time. Jet velocity is 33 m/s. Reynolds number $= 580$.

however, the exposure time of the premixed flame was increased from 0.09 to 4 s. This difference represents a factor of 45 increase in emission intensity with the diffusion H_2–air flame. For comparison, at the same aperture setting of $f2/4$, an exposure time of approximately 0.066 s was required to record the same exposure from a slightly lean, non-sooty, premixed CH_4 flame stabilized on a flat flame burner. Under non-sooty conditions this flame is blue in appearance, with the blue emission being primarily from CH^* chemiluminescence.

Emission spectra from the premixed H_2–air jet flame pictured in Fig. 4d identify the general spectral features of this flame. Fig. 5a shows the emission spectrum for the wavelength range extending from the ultraviolet to the near-infrared; Fig. 5b shows the calculated infrared emission spectrum for a diffusion H_2-jet flame [12]. The ultraviolet wavelengths below 400 nm are not visible to the human eye. The visible region extends from 400 to 750 nm, which covers emission appearing as blue, green, yellow, orange, and red. The infrared flame emission, consists of the near- (750 to 5000 nm) and far-infrared regions (above 5000 nm). As with ultraviolet light, the infrared region is not visible to the naked eye.

For hydrogen–air flames, the most notable emission features are from OH^* molecules in the ultraviolet wavelength range and from vibrationally excited H_2O molecules in the infrared region. In the infrared region, H_2O has strong emission bands at 1800, 2700 and 6300 nm. Flame emission from the infrared region dominates the total radiative emission from hydrogen flames. Additionally, emission from highly vibrationally excited H_2O [13] in the wavelength range from 600 to about 900 nm produces the red appearance seen over the entire length of the diffusion H_2 flame in Fig. 3 and in the downstream region of the premixed H_2/air flames in Fig. 4. A continuous blue emission region to the long-wavelength side of the OH peak in Fig. 5a is relatively weak and may be attributed to the reaction between OH and H radicals that combine to produce H_2O (see following discussion). This blue emission is visible in both the diffusion H_2 flame (Fig. 3) and near the base of the premixed H_2–air flame (Fig. 4).

Several tests were conducted to eliminate the possibility of gas impurities leading to the observed blue emission. For example, in

hydrocarbon flames blue emission is quite visible and known to be due primarily to electronically-excited CH^* located near 431 nm. Additionally CO_2^* produces a broad continuum. A potential source of carbon atoms is the presence of hydrocarbon impurities in the hydrogen fuel. To eliminate fuel impurities as a source of emission, spectra (not shown) were taken using both CP grade (99.0% H_2) and ultra-high purity (99.999% H_2). As noted previously, the maximum level of impurities in the CP grade and ultra-high purity grade was specified by the manufacturer as less than 1000 and 10 ppb, respectively. These impurities consist of N_2, O_2, H_2O and methane in decreasing order, with O_2 and H_2O being the most difficult to remove. No changes in the observed flame emission spectra were observed, indicating that carbon-containing impurities in the H_2 fuel are not responsible for the blue emission. Alternatively, impurities in the air, either entrained room air in the case of the diffusion flame or bottled air in the case of the premixed flame could provide a source of carbon to produce CH molecules in the high temperature flame. To eliminate hydrocarbon contamination and other sources of carbon in the air (CO_2 for example), a mixture of argon/oxygen was substituted for the air in the premixed flame and found to have no effect on the blue emission. Additionally, the premixed flame was operated with a low-velocity, surrounding guard flow of either pure nitrogen or pure argon to prevent entrainment of room air. Again no effect was observed on the blue emission. Finally, various levels of CO_2 were added to the reactants as a means of adding carbon atoms with no effect of flame emission. It was concluded that the source of the blue emission was not due to carbon-containing impurities in either the fuel or the air.

Nitrogen chemistry can also lead to visible emission in H_2/air flames. Previous studies have cited the observation of green emission from the $NO + O \rightarrow NO_2 + h\nu$ reaction [5,14]. To eliminate nitrogen chemistry as a potential source of chemiluminescence in the current experiments, emission from premixed $H_2/O_2/N_2$ and $H_2/O_2/Ar$ flames was compared, and no change in the structure of the emission spectrum was observed.

Thus we assert that the blue emission observed in the current experiments results from chemistry involving only H and O. Several previous studies in the literature have investigated the
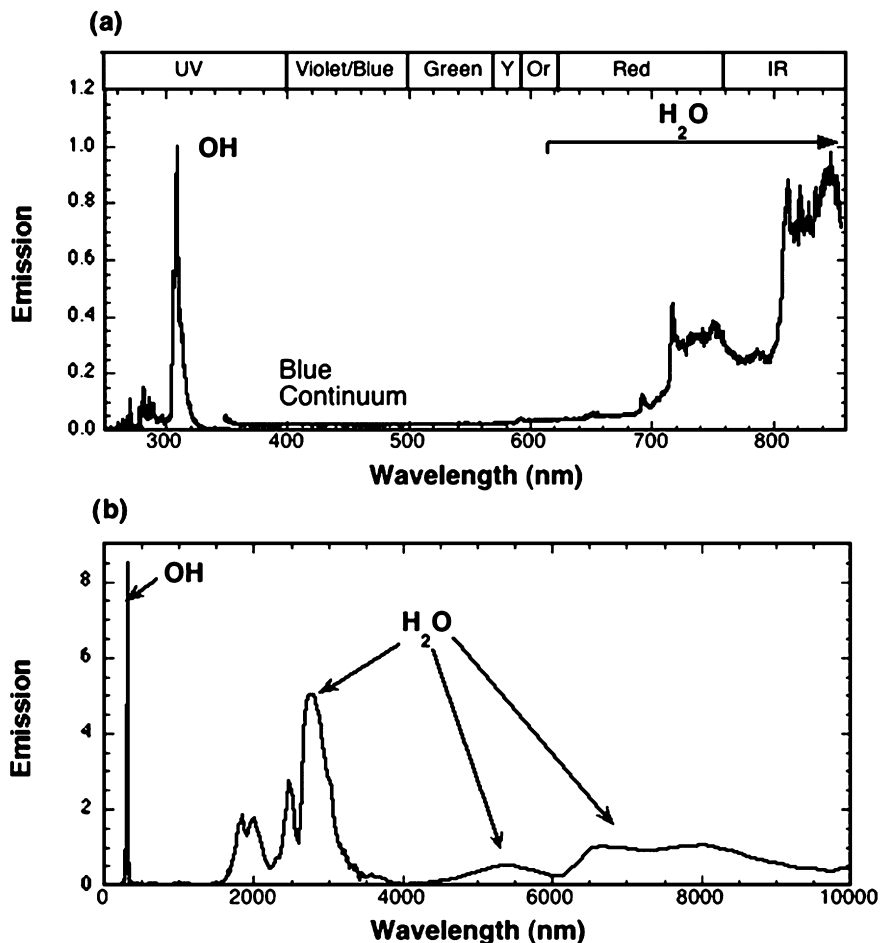
Fig. 5. Emission spectra in typical hydrogen–air flames: (a) premixed H_2–air jet flame showing measured spectral peaks from ultraviolet to near infrared; (b) diffusion H_2–air jet flame showing calculated spectral features in infrared range of wavelengths [12]. Note that the visible spectra extending from 350 nm to 850 nm in (a) was scaled by a factor of 6.5 with respect to the OH spectra in the ultraviolet.

source of the continuous blue emission in hydrogen flames. Generally, these studies concluded that the emission is attributable to reactions between flame radical species such as OH and H. The proposed emission mechanisms, however, still appear to be controversial. The two most likely proposed mechanisms are

$$OH + OH \rightarrow H_2O_2 + h\nu \tag{1}$$

and

$$OH + H \rightarrow H_2O + h\nu. \tag{2}$$

Observations of the pressure dependence of the emission intensity from hydrogen flames suggested that reaction (1) was more likely because the mole fraction of OH is less sensitive to pressure than the H atom [2]. Subsequent comparisons by Padley [3] of the temperature dependence of the emission with measured H and OH concentrations indicated that mechanism (2) was more likely. More recent measurements in H_2/NO flames by Vanpee and Mainiero [5], however, showed that flame emission decreased with flame hydrogen content, which is inconsistent with mechanism (2). Instead they found better agreement between the emission intensity and the square of the predicted OH concentration. However, as noted by Wormhoudt and Yousefian [6], the energy released from OH recombination is sufficiently small as to make the formation of H_2O_2 through reaction (1) an unlikely emission mechanism.

Recent discussions with researchers have yielded several alternative sources for the observed blue emission. For example, Nguyen and Rabinowitz [15] suggested two alternative sources of blue emission. The first is due to molecular H_2 lines in the region

410 to 477 nm [16]. The second involves emission from H atoms at 434.05 nm (2p–5d transition). Note that the higher-resolution spectra presented in the next section do not show any evidence of the isolated H-atom emission lines and thus rule out the second suggested source. Further work is clearly needed to explore these or other potential emission sources, or to identify which of reaction pathways (1) or (2) are responsible.

3.2. Spectra recorded with 2400-lpmm grating

Emission spectra were acquired using the 2400-lpmm grating to identify the finer spectral features of H_2 flame emission in the wavelength range over which the blue continuum is observed. Shown in Fig. 6 are emission spectra obtained in a premixed H_2/O_2 flame at an equivalence ratio of $\phi = 0.92$. In general, the emission intensity decreases by a factor of two between 410 and 510 nm. The inset shows an expanded view of the wavelength range between 412 and 432 nm. In the expanded view, one clearly observes distinct finer spectral features superimposed on a broadband continuum. The four separate spectral scans plotted in the expanded view superimpose well and indicate that these finer spectral features are reproducible and are not attributable to random noise. We further verified that the finer features are not due to fixed pattern noise in the detection system by rotating the grating by small steps and verifying that the spectral features shifted appropriately in the images. Gaydon [1] notes in a discussion of emission spectra in H_2/O_2 flames the superposition of numerous fine lines on a broadband blue continuum. He further notes that Wolfhard and
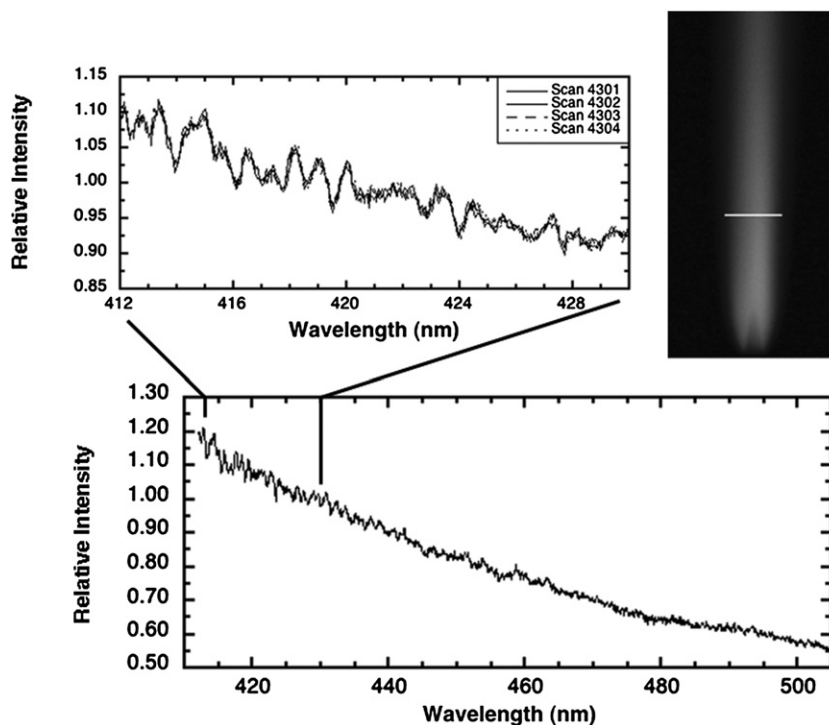
Fig. 6. Measured spectra in premixed H_2/O_2 jet flame with $\phi = 0.92$: (a) emission spectra collected with 2400-lpmm grating showing spectral peaks in region of blue broadband continuum between 412 to 510 nm. Insert shows expanded view with four spectral scans superimposed to show reproducibility. The white region in flame photograph shows the size and orientation of the collection volume.

Parker [17] attributed the fine lines to the Schumann–Runge system of O_2. However, a closer examination of the latter reference indicates that the O_2 lines are shifted toward the ultraviolet and do not appear in the blue continuum region. Based on relative intensity changes of the blue continuum and the O_2 bands observed in H_2–air flames, Diederichsen and Wolfhard [2] concluded that O_2 bands do not contribute to continuum emissions. Similarly, Vanpee and Mainiero [5] found in premixed H_2-rich, stoichiometric and O_2-rich flames that the O_2 bands need not be considered in any analysis of the blue continuum because no sensitivity of the broadband emission was seen as flame stoichiometry was varied.

Fig. 7 shows the effect of hydrocarbon addition on the spectral features in the premixed H_2/O_2 flame at $\phi = 0.92$. In addition to the pure H_2 fuel, methane is added in quantities varying between 0.93% and up to 10.8% by volume. Also shown in Fig. 7 is an emission spectrum from a pure CH_4 premixed flame. Note that in the CH_4 premixed flame, the spectra were recorded in the downstream, post-flame region to avoid the chemiluminescence from CH^* and CO_2^* that dominates flame emission in the vicinity of the flame front [18]. Although the amplitude of the broadband emission changes with varying CH_4 addition, Fig. 7a shows that the shape and slope of the broadband emission does not change, even when pure CH_4 replaces H_2 as the fuel. This observation brings into question if the broadband blue emission in the methane flame is solely due to CO_2^*. A close examination of the spectra for different CH_4 addition levels also indicates that the amplitude of the finer spectral peaks relative to the broadband emission decreases slightly with increased CH_4 addition. The spectra are re-plotted in Fig. 7b to demonstrate good correspondence between spectral peaks for the differing amounts of CH_4 addition. Here the underlying continuum was fitted with a smooth function, which was then subtracted from the measured spectrum to extract the finer structure. These results, taken together with spectra indicating that inclusion of carbon via CO_2 addition does not effect the spectral details of the finer structure (not shown), suggest that the flame chemistry resulting in the emission spectra observed are indepen-
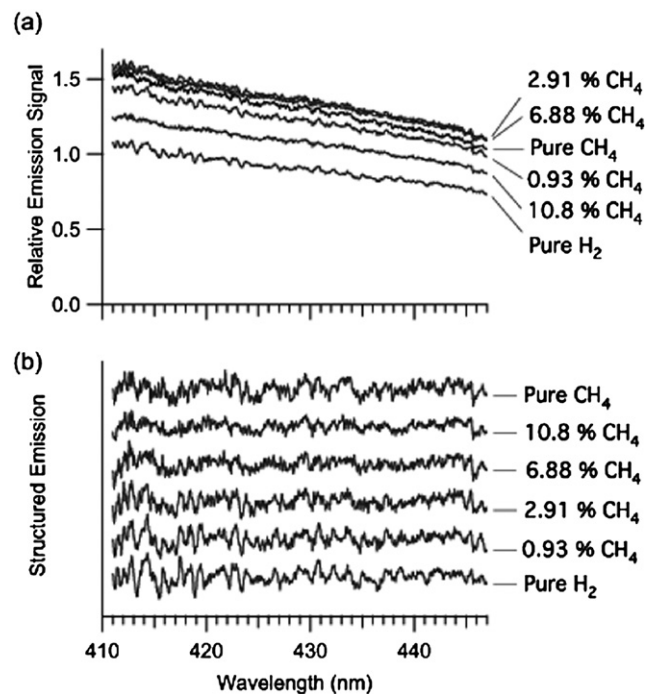

Fig. 7. (a) Measured spectra in premixed H_2/O_2 jet flame with various amounts of methane addition. (b) Same as (a) with background continuum subtracted to emphasize the finer structure of the spectrum.

dent of carbon chemistry. Similar emission spectra (not shown) obtained with and without nitrogen addition showed good correspondence, indicating that nitrogen chemistry has no effect of flame emission spectra.

The effect of flame temperature on the emission spectra in premixed $H_2/O_2/Ar$ jet flames is shown in Fig. 8. These spectra were obtained by varying the equivalence ratio and the amount of Ar
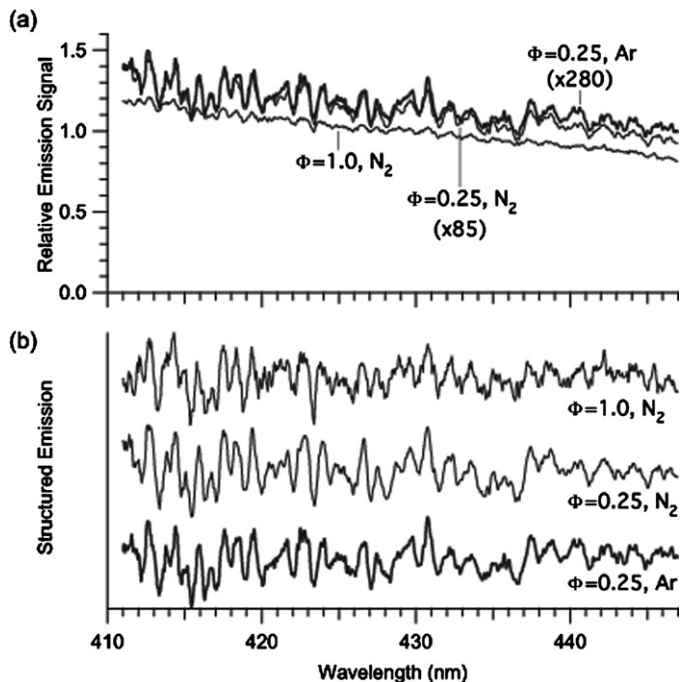
(a)

(b)

Fig. 8. (a) Measured spectra in premixed $H_2/O_2/Ar$ jet flames. ($-$) $\phi = 0.25$ with argon addition (Tad = 2390 K); ($-$) $\phi = 0.25$ with no diluent (Tad = 2500 K); ($-$) $\phi = 0.92$ with no diluent (Tad = 3079 K). (b) Same as (a) with background continuum subtracted to emphasize the finer structure of the spectrum.

dilution. Spectra are shown for equilibrium flame temperatures of 2400 K ($\phi = 0.25$, with Ar dilution), 2500 K ($\phi = 0.25$, no Ar dilution) and 3100 K ($\phi = 0.92$, no Ar dilution). Fig. 8a shows that the magnitude of the broadband emission increases with flame temperature in a highly nonlinear manner. For example, as the temperature increases from 2400 to 2500 K, the broadband continuum intensity increases by a factor of about 85. For the increase from 2400 to 3100 K, the increase is nearly a factor of 280. These increases are constant across the entire wavelength range of 412 to 446 nm shown. It is also evident that the intensity of the finer spectral structure relative to the underlying continuum is comparable in the two $\phi = 0.25$ flames but is much less in the $\phi = 0.92$ flame. Fig. 8b shows these spectra after subtracting a fit to the continuum background. The data verify that the amplitude and shape of the finer spectral structure is independent of flame temperature, with good peak overlap at all three temperatures.

Vanpee and Mainiero [5] attributed an observed increase in continuum intensity in H_2/O_2 diffusion flames primarily to increased radical concentrations (OH and H) and not an increase in temperature. This was established by increasing the O_2 content in the shroud flow surrounding a diffusion H_2 flame. The Ar/O_2 ratio in the shroud flow was varied from 3.17 to 0.0. Although this variation resulted in a relatively small increase in flame temperature (2712–3078 K), the OH radical concentration increased by nearly a factor of five. The correspondingly large factor of 500 increase in continuum intensity confirmed the primary dependence on radical concentration. (It was further noted that the factor of 500 increase in intensity was attributable in part to an increased in flame length with Ar dilution.) In agreement with the present results, the continuum distribution remained essentially the same for all flames, although a small temperature effect was noted in the highest temperature flame where the continuum intensity increases more at shorter wavelengths than at longer wavelengths between 375 to 550 nm. In the current work, the slopes of the spectra for the three flames in Fig. 8a, however, remain constant over the relatively narrow wavelength range shown.
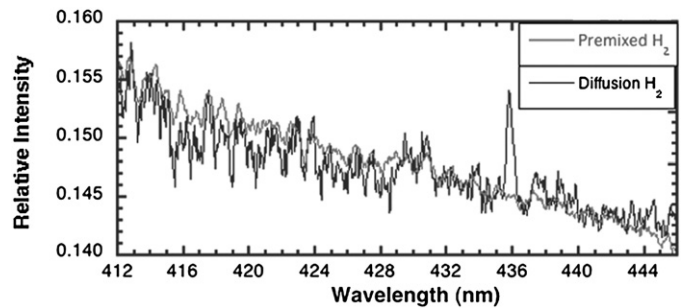

Fig. 9. Measured spectra in hydrogen jet flames. (a) Premixed H_2/O_2 flame at $\phi = 0.92$; (b) H_2/air diffusion flame. (The feature at 436 nm in the diffusion flame spectrum is a mercury line characteristic of fluorescence tube lighting, and we expect this artifact was caused by unintentional exposure to room lights.)

The present data can also be compared with the variation in continuum intensity with temperature measured in premixed $H_2/O_2/N_2$ flames by Padley [3]. Based on a fit to their data, the estimated intensity increase between flame temperatures of 2400 and 2500 K is 1.34, and between 2500 and 3100 K it is 2.73, which is considerably less than measured in the present investigation. This discrepancy can perhaps be attributed to the necessary extrapolation of their data fits from the lower temperature range of 1785–2439 K. Also, the wavelength at which their measurements were taken of 490 nm is considerably higher than the range of 412–446 nm in the present study.

A comparison of spectra obtained in the premixed H_2/O_2 jet flame at $\phi = 0.92$ and a diffusion H_2 jet flame into air is shown in Fig. 9. The same spectral structure is seen in both flames. The fine scale structure shows good correspondence in peak locations, although the amplitude of the finer spectral peaks relative to the broadband emission is higher in the diffusion flame.

4. Conclusions

Flame spectra are presented to characterize emission bands from hydrogen flames in the ultraviolet, visible and infrared regions of the spectrum. The emission bands due to water, and a blue continuum result in a visible hydrogen flame. While visible emissions from hydrogen flames are considerably weaker than those from comparable hydrocarbon flames, they are visible at reduced light levels in most cases. Detailed spectra are obtained to characterize the visible blue emission. The spectra indicate that fine spectral structure is superimposed on a broadband continuum extending from the ultraviolet into the visible region. Tests were performed to show that this emission does not arise from carbon or nitrogen. The magnitude of the broadband emission increases nonlinearly with flame temperature while the finer spectral structure is insensitive to temperature. The results show that the fine scale structure is comparable in both diffusion and premixed H_2 flames.

References

[1] A.G. Gaydon, The Spectroscopy of Flames, Chapman and Hall, London, 1974.

[2] J. Diederichsen, H.G. Wolfhard, Proc. R. Soc. London, Ser. A 236 (1956) 89–103.

[3] P.J. Padley, Trans. Faraday Soc. 56 (1960) 449–454.

[4] N.V. Mossholder, V.A. Fassel, R.N. Kniseley, Anal. Chem. 45 (1973) 1614–1626.

[5] M. Vanpee, R.J. Mainiero, Combust. Flame 34 (1979) 219–220.

[6] J. Wormhoudt, V. Yousefian, J. Spacecraft 19 (1982) 382–384.

[7] R.W. Schefer, T.D. Smith, C.J. Marek, Evaluation of NASA Lean Premixed Hydrogen Burner, Report SAND2002-8609, Sandia National Laboratories, January 2003.

[8] L.C. Haber, U. Vandsburger, Combust. Sci. Technol. 175 (2003) 1859–1891.

[9] A.G. Gaydon, H.G. Wolfhard, Flames: Their Structure, Radiation and Temperature, 4th ed., Chapman and Hall, London, 1978.

[10] H.N. Najm, P.H. Paul, C.J. Mueller, P.S. Wyckoff, Combust. Flame 113 (1994) 312–332.

[11] Y. Ikeda, J. Kojima, H. Hashimoto, Proc. Combust. Inst. 29 (2002) 1495–1501.

[12] J.H. Frank, R.S. Barlow, C. Lundquist, Proc. Combust. Inst. 28 (2000) 447–454.

[13] A.G. Gaydon, Proc. R. Soc. London, Ser. A 181 (1942) 197–209.

[14] A.G. Gaydon, Proc. R. Soc. London, Ser. A 183 (1944) 111–124.

[15] Q. Nguyen, M. Rabinowitz, Personal communication, NASA Glen Research Center, Cleveland, OH, 2005.

[16] J.K.L. MacDonald, Proc. R. Soc. London 131 (1931) 146–152.

[17] Wolfhard, Parker, Proc. Phys. Soc. London, Sect. A 62 (1949) 722–730.

[18] J.-M. Samaniego, F.N. Egolfopoulos, C.T. Bowman, Combust. Sci. Technol. 109 (1995) 183–203.